Effects of agitator blade scaling on mixing in dissolving tanks

PATRICK GAREAU, MARKUS BUSSMANN, AND NIKOLAI DEMARTINI

ABSTRACT: Hard calcium carbonate scale often forms on the agitators in smelt dissolving tanks. The effects of this scale on mixing are not well understood. While mixing in tanks has often been modeled in the literature, there have been no studies involving agitator scaling.

To better understand the impact of agitator scaling on hydrodynamics and tank concentrations, a steady state, three-dimensional (3D) model has been developed for a smelt dissolving tank at a kraft pulp mill. In this work, four cases are compared: an agitator with no scaling, mild scaling, moderate scaling, and extreme scaling. The extreme scaling case is representative of scale buildup on a dissolving tank agitator that was significant enough that the agitator had to be stopped and cleaned. The reduction in the agitator fluid jet velocity is relatively small for the mild and moderate scaling cases, but it becomes more significant for the extreme scaling case, for which the results indicate that the mixing of the smelt with the weak wash is likely poor and that there would thus be a risk of smelt pooling.

Application: A smelt dissolving tank model has been developed to predict how tank hydrodynamics and smelt concentrations respond to the presence of agitator scaling.

Causticizing plants in kraft pulp mills frequently suffer from hard calcium carbonate scale formation on the smelt dissolving tank agitators, walls, and floor, as well as in the downstream pumps, pipelines, and other green liquor handling equipment [1]. As scale builds up on an agitator, it can eventually bridge between the blades. The scaling illustrated in **Fig. 1** is an example of extreme scaling in which the agitator had to be shut down, removed, and cleaned because it was no longer possible to maintain the required rotational speed without significant vibrations and very high pump amps. The scale in this case is thickest near the center of the agitator, whereas the blade tips are relatively clean. Scaling also covers the shaft. Although a certain amount of scale will inevitably build up on the agitators, unmanaged scaling may cause insufficient tank mixing, in addition to vibrations due to mass imbalance, increased motor load due to the mass of the scale, and damage to the agitator packing or mechanical seal. For side wall agitators, damage to the packing or seal leads to reliability and safety issues. While many tanks have backup steam agitators to deal with agitator failure, these are only a short-term solution, as it is not known how long tanks can be operated under these conditions.

In a smelt dissolving tank, droplets of shattered molten smelt from the recovery boiler fall into the tank, interact with weak wash, and dissolve to produce green liquor. Agitators promote the mixing in the tank, which is critical to rapid dissolution of the smelt and ideally prevents the smelt from settling to the bottom of the tank. Good smelt dissolution and avoidance of smelt pooling is needed to avoid loud, violent, and potentially dangerous smelt-water interactions, such as during smelt runoffs [2,3].

1. Severe agitator scaling.

Cho [4] recently studied the effects of agitator configurations on the hydrodynamics and outlet concentrations in a cylindrical smelt dissolving tank to determine ideal design and operating conditions. That study used MixIT, a commercial computational fluid dynamics (CFD) software for simulating tank mixing. It was found that positioning agitators away from the outlet reduces outlet concentration fluctuations and low-velocity regions (i.e., "dead zones") where smelt might pool. It also indicated that tanks with three

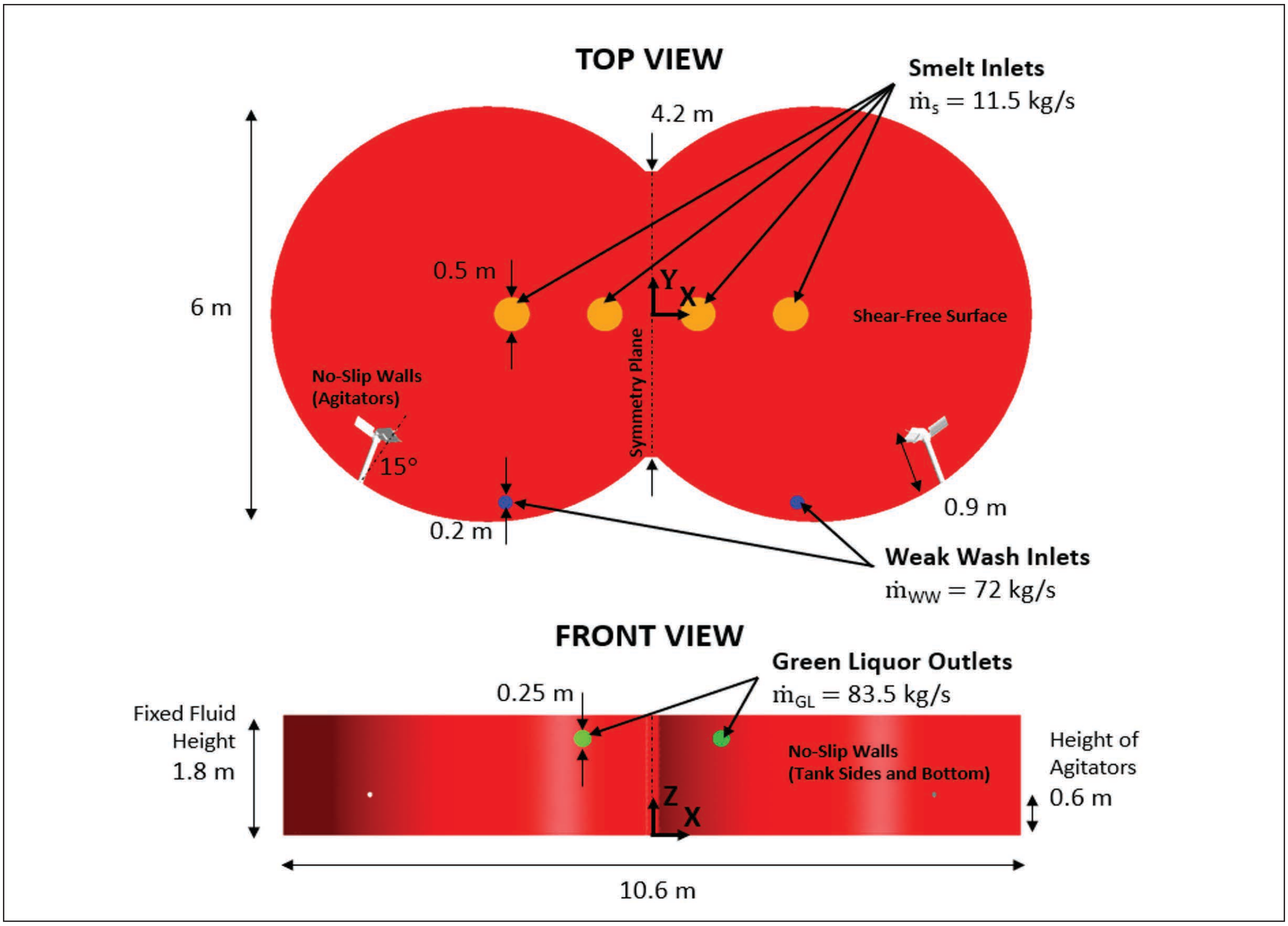

2. Model geometry and boundary conditions.

impellers could perform better than tanks with only two, although a poorly configured three-impeller tank could perform worse than a well configured two-impeller tank.

Although no other numerical studies of mixing in smelt dissolving tanks were found in literature, there have been several numerical studies of mixing tanks in general, usually involving cylindrical tanks with either top-entry [5-9] or side-entry [10-12] agitator configurations. The topics and purposes of these studies are all widely varied. For example, Madhania et al. [10,12] compared different turbulent and mixing model couplings for the mixing of two miscible liquids with large viscosity differences in a conical-bottomed cylindrical tank and the resulting mixing times obtained with the standard and realizable k-ε turbulence models. Torotwa and Ji [5] compared flow and homogeneity for four impeller designs (anchor, sawtooth, counterflow, and Rushton turbine). Zamankhan [6] studied the dissolution of multi-sized sodium formate granules in a baffled laboratory-scale tank. Hernández-Jaramillo et al. [11] simulated flow distribution in a crude oil storage tank. Zadravec et al. [9] examined the effect of the rotating domain size in a multiple reference frame modeling approach on numerical accuracy compared to experimental results. Cao et al. [7] developed a model for predicting the dissolution of spray-dried detergent powder, linking the dissolution behavior of bulk particles to the input power of the mixing system. Finally, Pakzad et al. [8] characterized the performance of a Scaba 6SRGT impeller for the mixing of non-Newtonian pseudoplastic fluids with a yield stress in laminar and transitional flow regimes.

The turbulence and mixing models that are used impact the numerical accuracy and computational cost. The Multiple Reference Frame model [13] was frequently used in the previously mentioned studies [5,8,9,10-12]. It is less accurate than the alternative Sliding Mesh model [14], but it is much less computationally expensive and allows for time-averaged steady-state solutions. Turbulence models included the standard k-ε [5,10,12]; realizable k-ε [10,12]; RNG k-ε [11]; k-ω-based shear stress turbulence [9]; and large-eddy simulation [6,10], with the latter being the most computationally expensive.

The objective of this work was to develop a CFD smelt dissolving tank model to determine how agitator scaling affects the hydrodynamics in the tank. Four cases are compared that range in degree of agitator scaling: clean agitators (i.e., no scaling), mild scaling (no bridging between blades), moderate scaling (bridging between blades), and extreme scaling (bridging between blades and more cover-

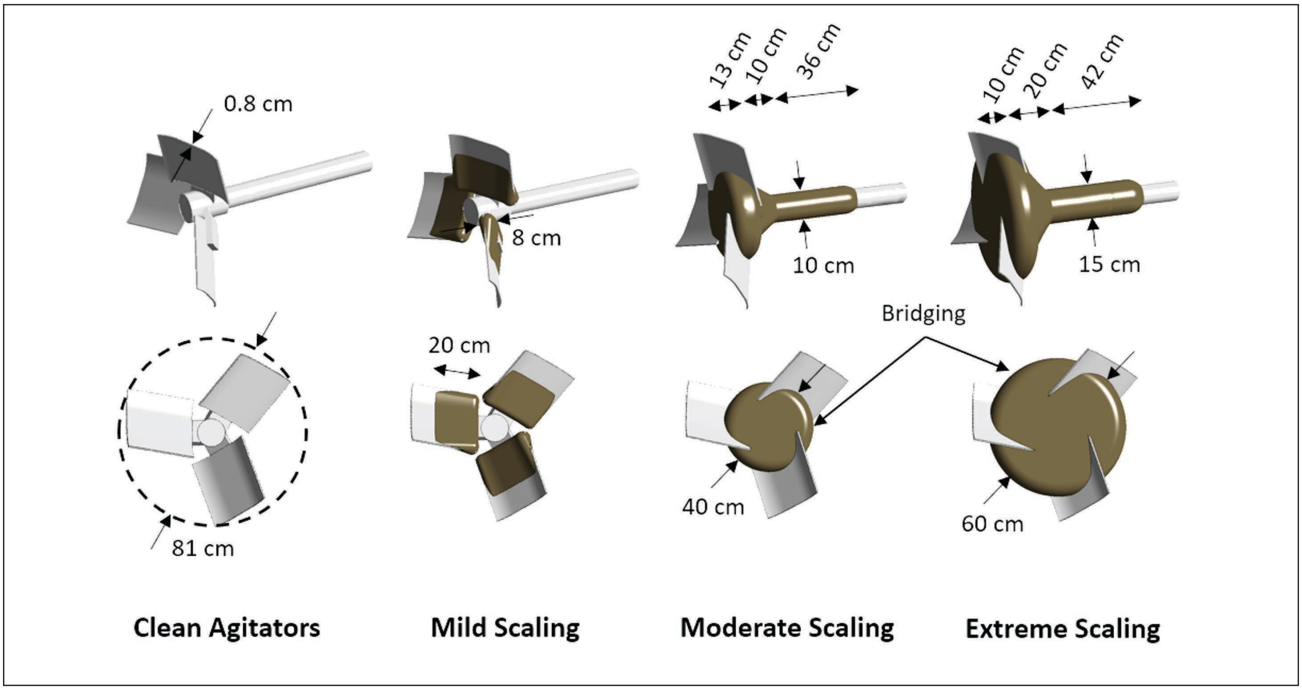

3. Agitator and scaling geometry.

age of blades). Velocity profiles for the four cases provide an indication of the extent to which mixing is affected. As described in the next section, smelt is treated as a liquid stream with twice the density of water [15], and then the density of the mixture of the weak wash and smelt are used to identify areas of relatively poor mixing.

COMPUTATIONAL METHODOLOGY

A steady state, three-dimensional (3D) model has been developed for a uniquely shaped industrial dissolving tank with side-entry agitators (**Fig. 2**). The tank resembles a peanut shell from above. Only the inside of the tank (i.e., the fluid domains and agitators) was modeled. The maximum length and width of the computational domain are 10.6 m and 6 m, respectively. A fixed height of 1.8 m was assumed for the fluid. Smelt was treated as a liquid miscible with water. Four smelt inlets, with a combined mass flow rate of $\dot{m}_S$= 11.5 kg/s, and two weak wash inlets, with a combined mass flow rate of $\dot{m}_{WW}$ = 72 kg/s, are located on the top surface of the domain. Two green liquor outlets, with a combined mass flow rate of $\dot{m}_{GL}$= 83.5 kg/s, are located on the front wall of the tank. The following material properties were assumed for weak wash and smelt: $\rho_{WW} = \rho_{water} = 1000$ kg/m^3, $\rho_{smelt} = 2\rho_{water} = 2000$ kg/m^3, and $\mu_{WW} = \mu_{smelt} = \mu_{GL} = 9.637\times10^{-3}$ kg/m-s. Shear-free conditions were imposed on the free surface and no-slip conditions on the tank walls and agitators. The agitators are offset 15° from the wall normal and are located 0.6 m from the bottom of the tank.

The geometry of the agitators and scaling from each case are given in **Fig. 3**. The mild scaling case has equal amounts of scaling on each blade that are thickest near the shaft of the agitator and then taper off about halfway up the blades. For the moderate and extreme scaling cases, the scale bridges the blades and covers the shaft. The extreme scaling case approximates the scaling shown in Fig. 1.

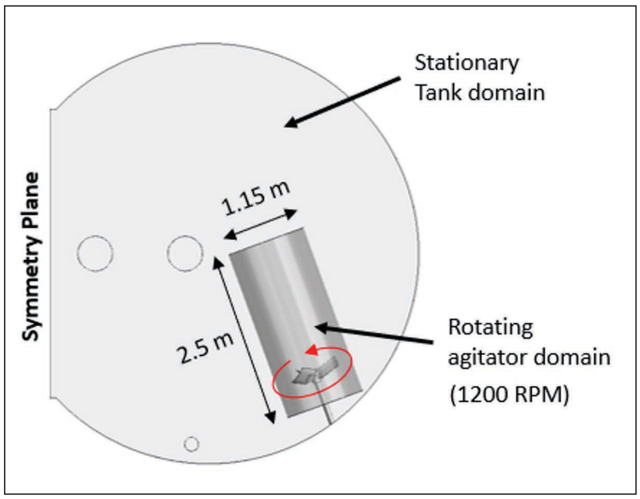

4. Multiple reference frame model setup.

The commercial, trademarked CFD software ANSYS Fluent was used to run the simulations. Preliminary simulations of the entire tank confirmed a symmetry about the tank center, and so thereafter, we modeled just the right half of the tank to reduce computational costs. Mixing was modeled with the Multiple Reference Frame model [13]. **Figure 4** shows the model setup. The tank was separated into a rotating agitator domain and a stationary domain for the remainder of the tank. Flow was solved in each subdomain in its corresponding reference frame. The rotating domain rotates at the speed of the agitator, 1200 rpm,

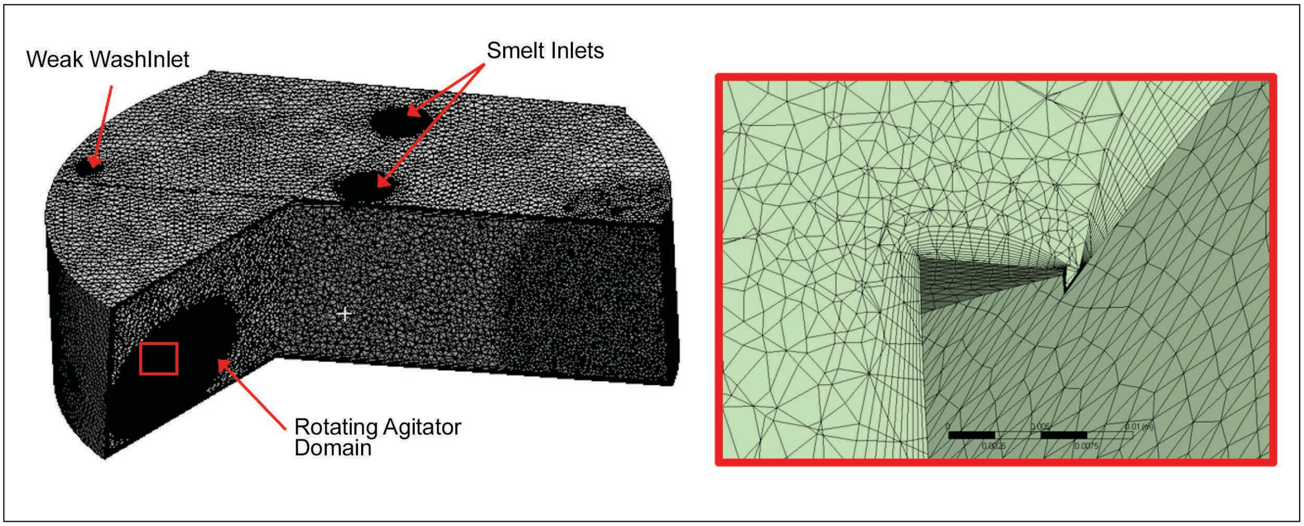

5. Cut-out view of the extreme scaling case mesh (left) and a zoom-in view of the agitator surface (right) prior to conversion to a polyhedral mesh.

which was kept constant even with scale up, as is done in practice. Although the rotating domain diameter was maximized to improve model accuracy, as was found in [9], the bottom of the tank posed an upper limit.

The realizable k-ε model was used to model turbulence. This model is a variation of the standard k-ε model and is more suitable for flows featuring strong streamline curvature, vortices, and rotation [16]. The curvature correction option and Menter-Lechner wall treatment were also used (see [16] for more information on turbulence modeling). For simplicity, the complex smelt-weak wash interaction described in [2,3] was not modeled.

Smelt concentration in the tank was modeled with the homogeneous multiphase mixture fraction model using an implicit formulation for the volume fractions of the miscible weak wash and smelt phases and the dispersed interface option because of the low loading of the smelt phase and to reduce computational cost (see [17] for more information on multiphase modeling).

The governing equations were spatially discretized in ANSYS Fluent with the following schemes: PRESTO! for pressure, second order upwind for momentum and turbulence, and QUICK for the multiphase volume fraction. The pressure-based solver and the SIMPLEC pressure-velocity coupling scheme were used. See [18] for detailed solver theory.

RESULTS AND DISCUSSION

Mesh independence and a convergence study

Meshes composed of tetrahedral cells were constructed for the right-half domain of each case using ANSYS Meshing. For example, **Fig. 5** shows the mesh used for the extreme scaling case. The mesh was refined at the inlets and outlet, the interfaces between rotating and stationary domains, and the agitator. Local refinements were also made within the rotating domain and the jet impingement region on the wall opposite the agitator. Mesh inflation was used on the walls

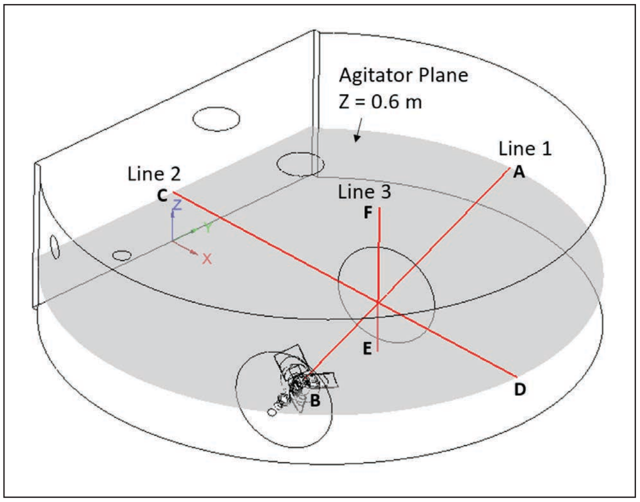

6. Three lines along which velocities are compared. Line 1 is co-linear with the agitator rotational axis. Line 2, also residing in the agitator plane, spans from the tank center to the opposite side wall. Line 3 is perpendicular to the agitator plane and passes through the intersection point of Lines 1 and 2.

and agitators (5 and 10 layers, respectively). Polyhedral meshes tend to be more efficient than tetrahedral meshes [19]; thus, once imported into ANSYS Fluent, the tetrahedral meshes were converted to meshes composed of polyhedral cells using the built-in Fluent conversion feature, reducing cell count by a factor of approximately 5. The prism cells in the inflation layers were preserved in the process.

A mesh study was conducted on the extreme scaling case to determine an appropriate level of mesh refinement, which was assumed to then apply for all the other cases. Three polyhedral meshes were compared: A, B, and C with 1.99 M, 3.71 M, and 6.29 M cells, respectively. To compare the three cases, velocities were examined along three lines illustrated in **Fig. 6**. **Figures 7–9** show the fluid velocities along those lines. Mesh independence is not fully

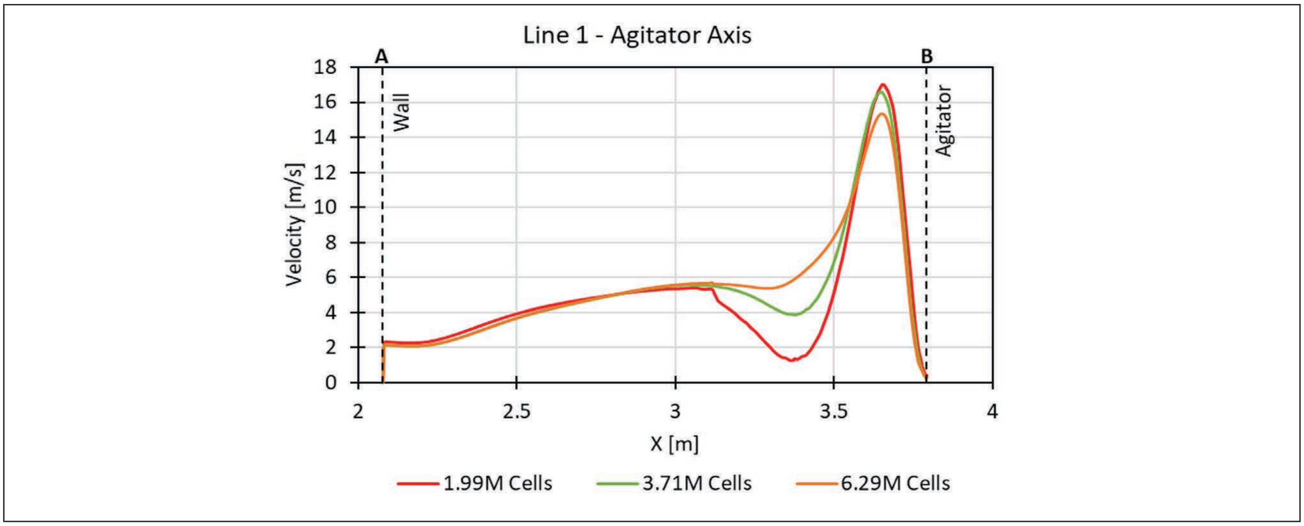

7. Mesh study velocity comparison along Line 1 from Fig. 6.

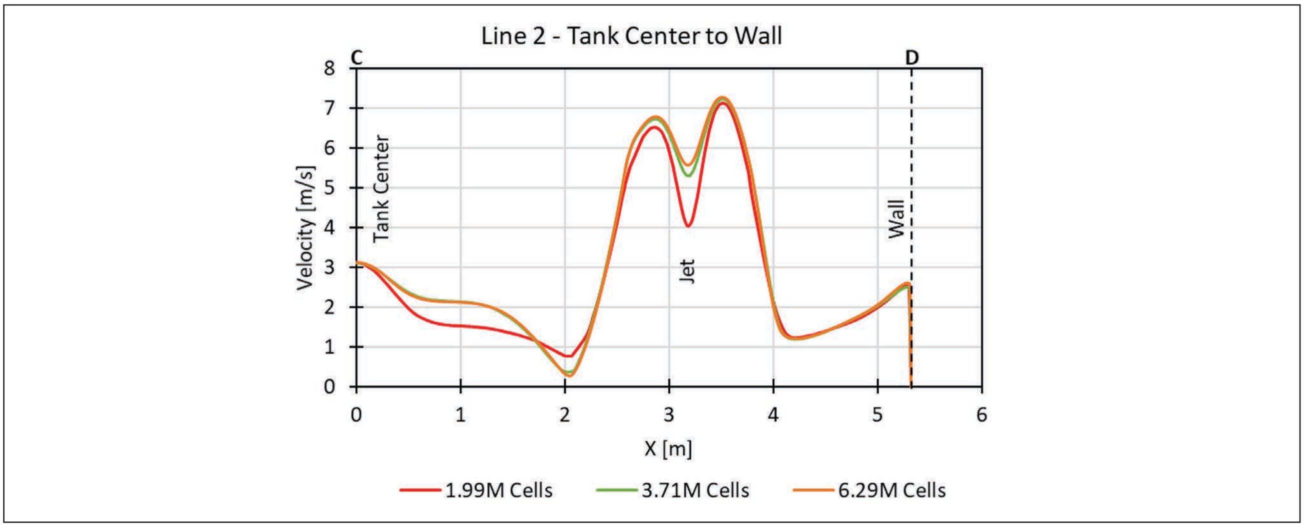

8. Mesh study velocity comparison along Line 2 from Fig. 6.

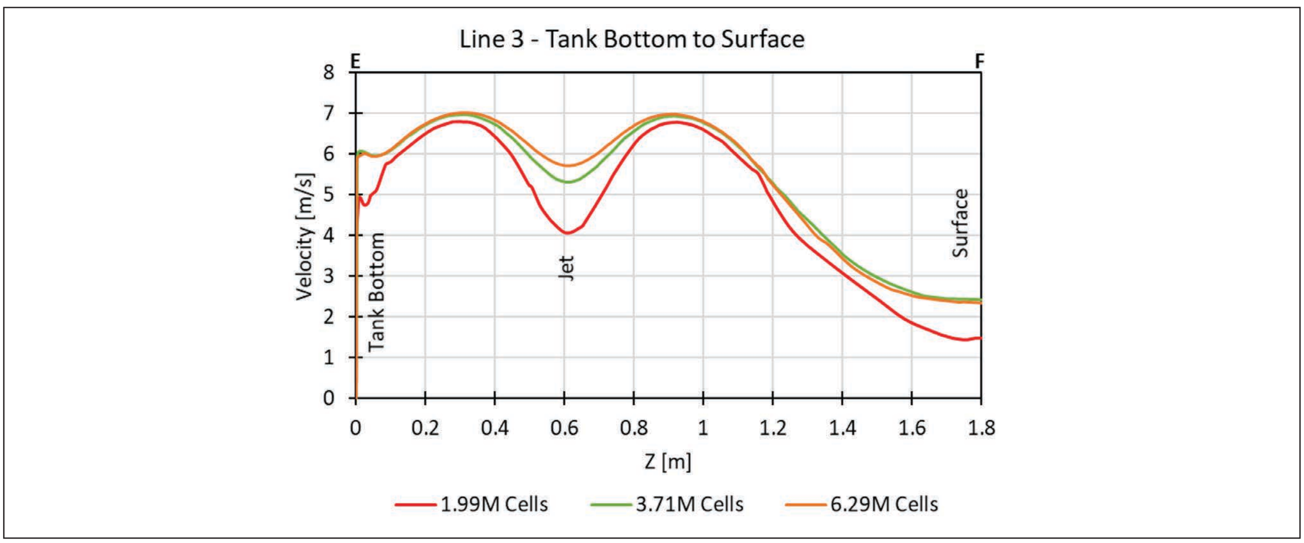

9. Mesh study velocity comparison along Line 3 from Fig. 6.

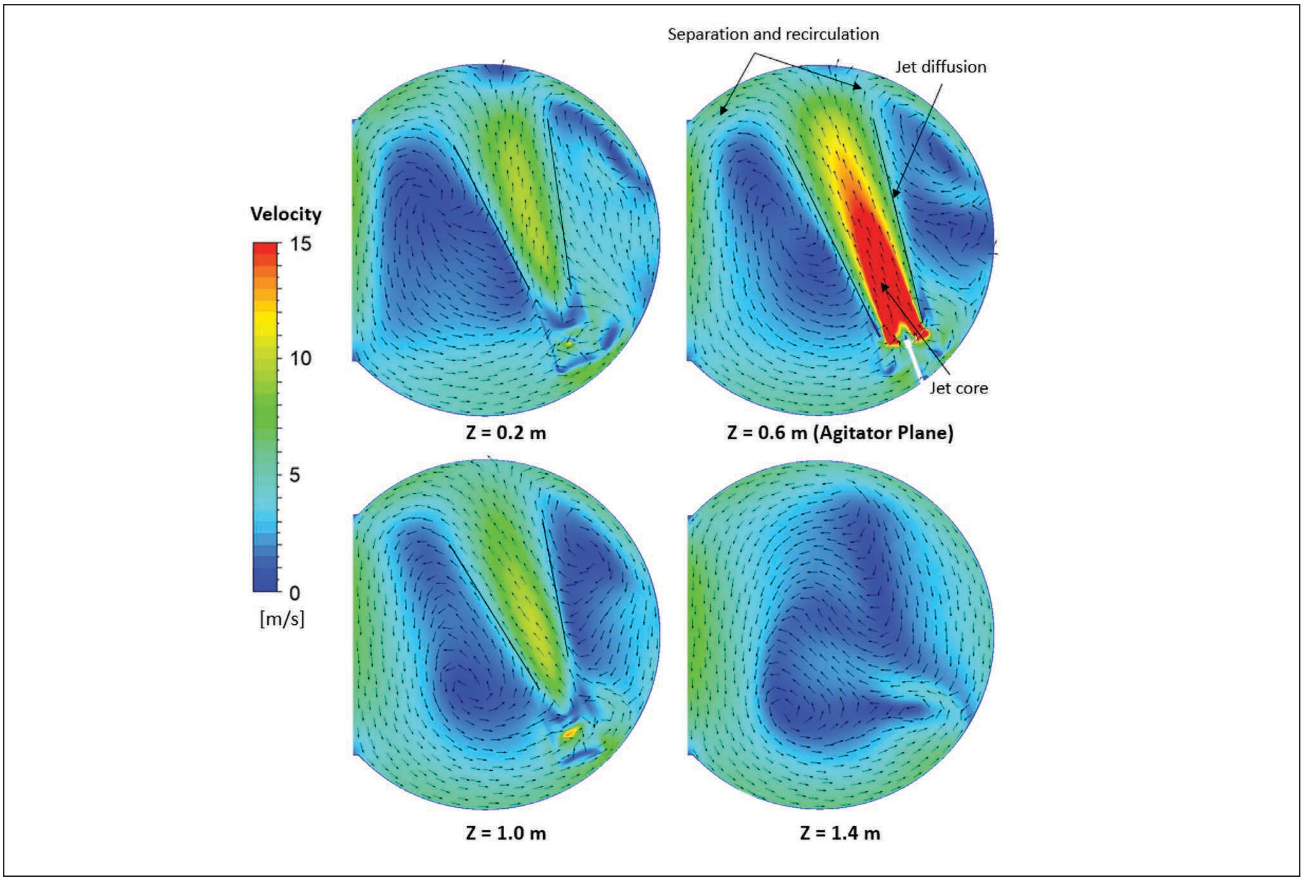

10. Clean agitator flow fields at Z = 0.2, 0.6, 1.0, and 1.4 m elevations from the bottom of the tank.

reached with Mesh B (3.71 M cells), as can be seen when comparing meshes B and C. Nevertheless, it was decided to proceed with this level of mesh refinement for the scaling study, because simulations took significant amounts of time to run and reach convergence. Based on these results, mesh-related inaccuracy is expected to be highest near the agitators but minimal throughout most of the tank.

Although there were no problems in achieving convergence for the extreme scaling case and clean agitator case, there were oscillations in the solutions for the other two cases, despite significant efforts to remove them. For example, modifying the turbulence model would sometimes resolve the issue for one case but create issues for others. It was ultimately decided to accept the oscillations, since velocities would only fluctuate locally within ±10% or less. Results for the mild and moderate scaling presented in what follows are the mean of these oscillations.

Scaling study

<u>Effects on velocity</u>

The clean agitator creates a high velocity jet that diffuses outward radially as it moves away from the agitator and impinges on the wall facing it (**Fig. 10**). The jet then separates and recirculates along the walls back toward the agitator, and some of the recirculated flow is drawn back into the jet. Eddies can be seen in the dark blue low-velocity regions. The agitator axis is at Z = 0.6 m and highest velocities are naturally seen at this level. At Z = 0.2 m and Z = 1.0 m, similar flow fields are obtained, although the jet is more diffuse and has a lower velocity due to the distance from the jet core. In these planes, the flow in the jet is also skewed to the right and left, respectively, due to the counterclockwise rotation imposed by the agitator. At Z = 1.4 m, the jet is very diffuse, although the recirculating flow pattern from the jet impingement is still present.

Figures 11 and 12 show similar flow fields for all the degrees of agitator scaling. The scaling reduces the jet velocity, as is apparent by the shorter high velocity red regions in the jet core at Z = 0.6 m with increased scaling. The regions outside of the jet also have lower velocities for the extreme scaling case compared to the other three, at both Z = 0.6 m and 1.0 m.

The average velocities in the tank (**Table I**) can be used to quantify the global impact of scaling on the dissolving tank hydrodynamics. With clean agitators, the average velocity in the tank is 4.00 m/s. This is reduced by 2.5%, 6.2%, and 35.2% due to mild, moderate, and extreme scaling, and so the overall effect is only pronounced for the extreme scaling case. It is interesting to note that the mild and moderate cases impact the velocities in similar ways, despite the bridging that is pres-

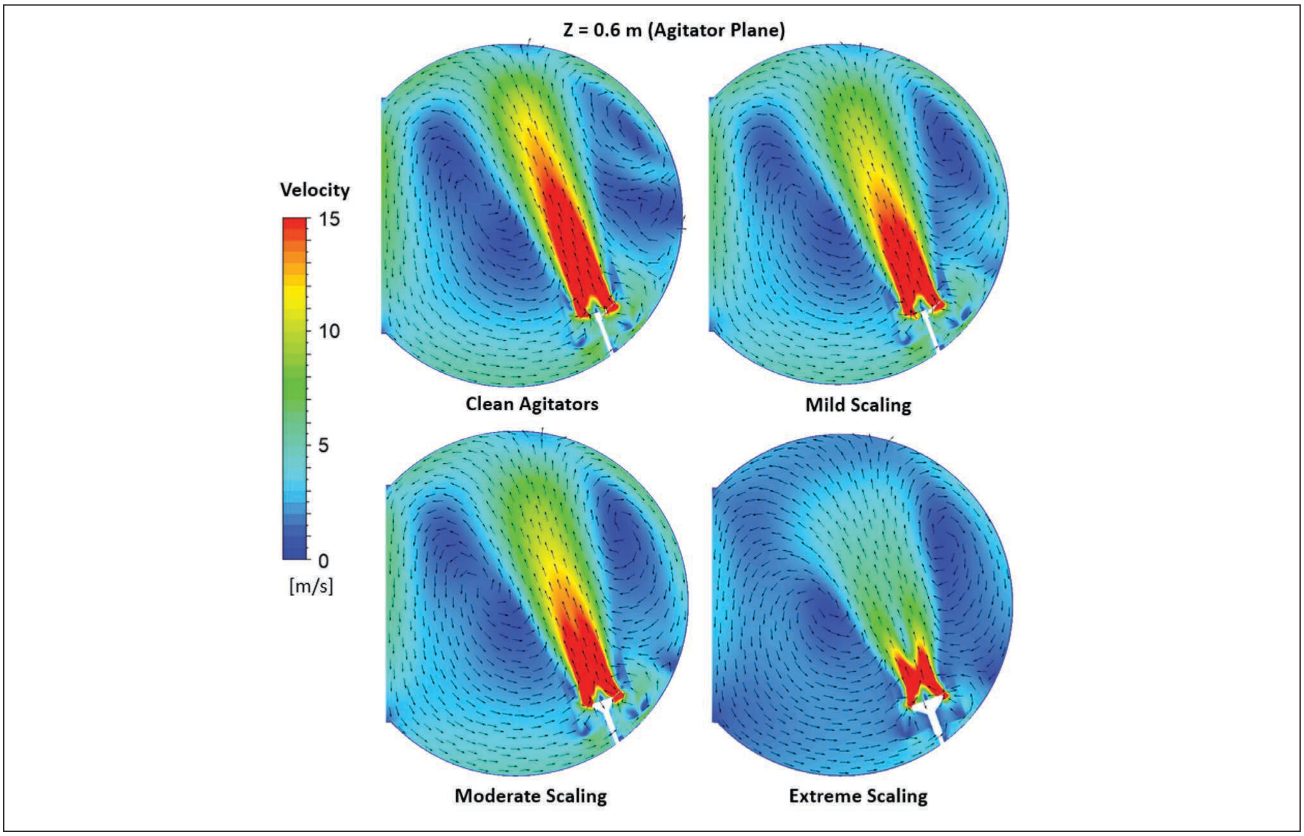

11. Flow field comparison of each scaling case at an elevation of Z = 0.6 m from the bottom of the tank (i.e., the agitator plane).

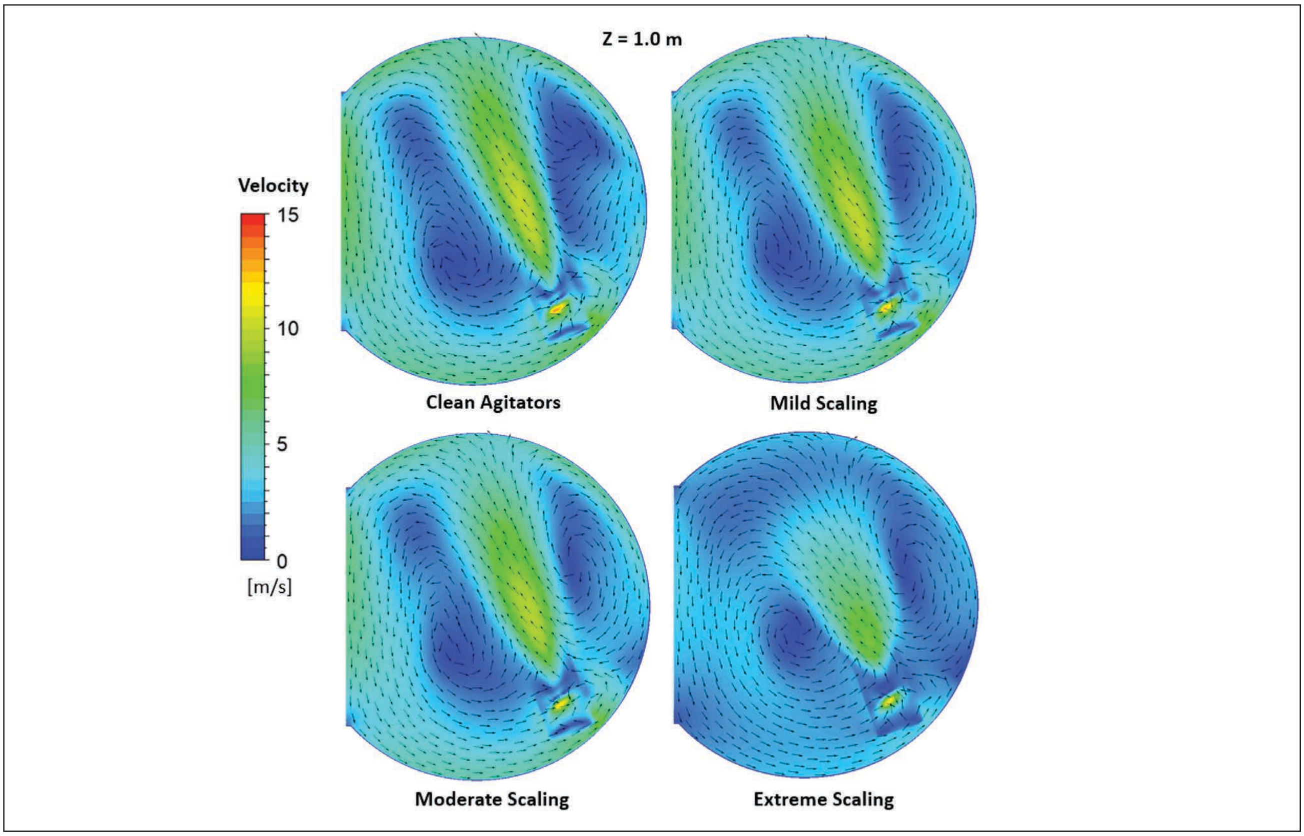

12. Flow field comparison of each scaling case at an elevation of Z = 1.0 m from the bottom of the tank.

Case:	Clean Agitator	Mild Scaling	Moderate Scaling	Extreme Scaling
Tank average velocity, m/s	4.00	3.90	3.75	2.59
Velocity reduction, %	--	2.5	6.2	35.2

I. Reduction of average velocities in the tank from scaling.

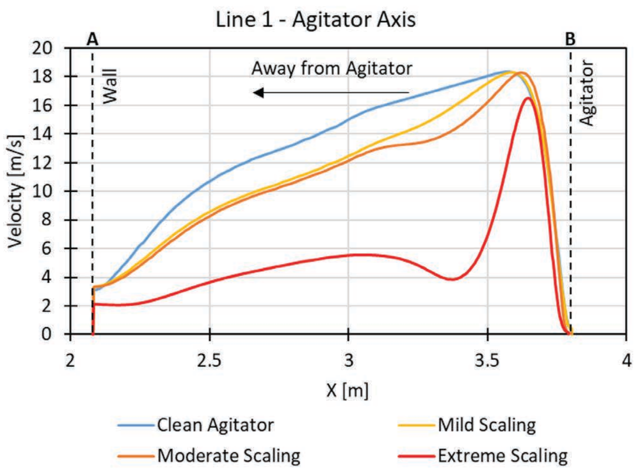

13. Velocity comparison of each scaling case along Line 1 from Fig. 6.

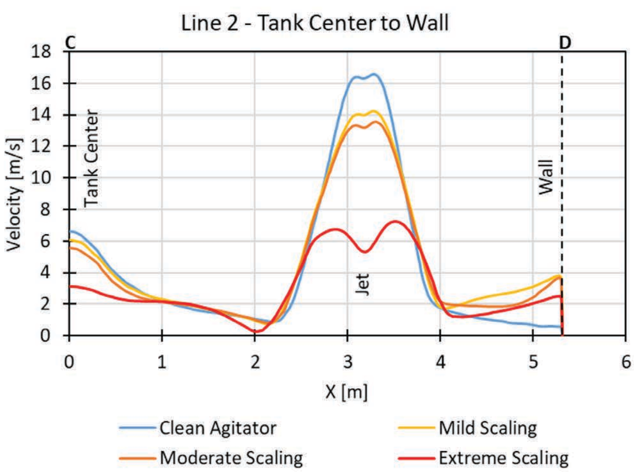

14. Velocity comparison of each scaling case along Line 2 from Fig. 6.

ent on the moderate scaling case. The similarity could be due to the relatively small blade spans in either case.

To quantitatively compare the four cases, velocities are plotted along Lines 1-3 from Fig. 6 shown earlier (**Figs. 13–15**). The peak jet velocity near the agitator at X = 3.79 m is similar for all four cases: ~16.5 m/s for the extreme scaling case and ~18.3 m/s for the other three cases (Fig. 13). The velocity decays very rapidly by X = 3.4 m for the extreme scaling case, whereas the other three cases show a more gradual velocity gradient along the line.

Perpendicular to the jet, velocities are generally lower as the scaling increases, particularly within the jet (**Fig. 14**). It is interesting to note that this is not the case near the wall, where velocities are higher with some scaling (the mild scaling case has the highest local velocity).

The effect of scaling on the diffusion of the jet is pronounced when looking at the vertical axis line, which is 1.79 m from the agitator (**Fig. 15**). Velocities are all very similar near the bottom of the tank. Near the free surface, the velocity is about the same for the clean agitator, mild, and moderate scaling cases, ~0.8 m/s, whereas it is higher for the extreme scaling case, ~2.4 m/s.

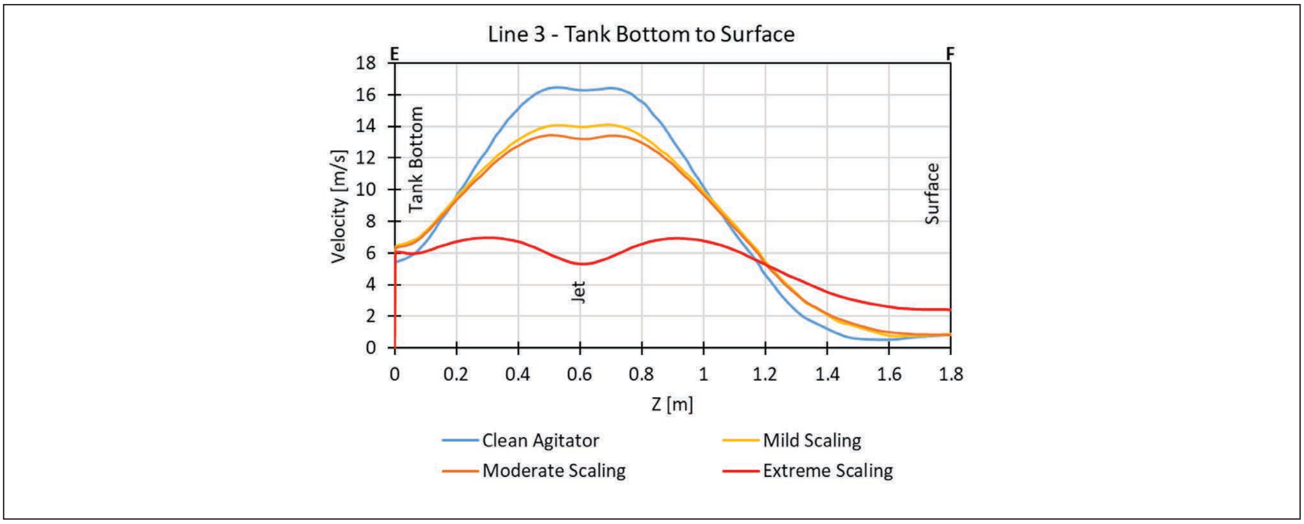

15. Velocity comparison of each scaling case along Line 3 from Fig. 6.

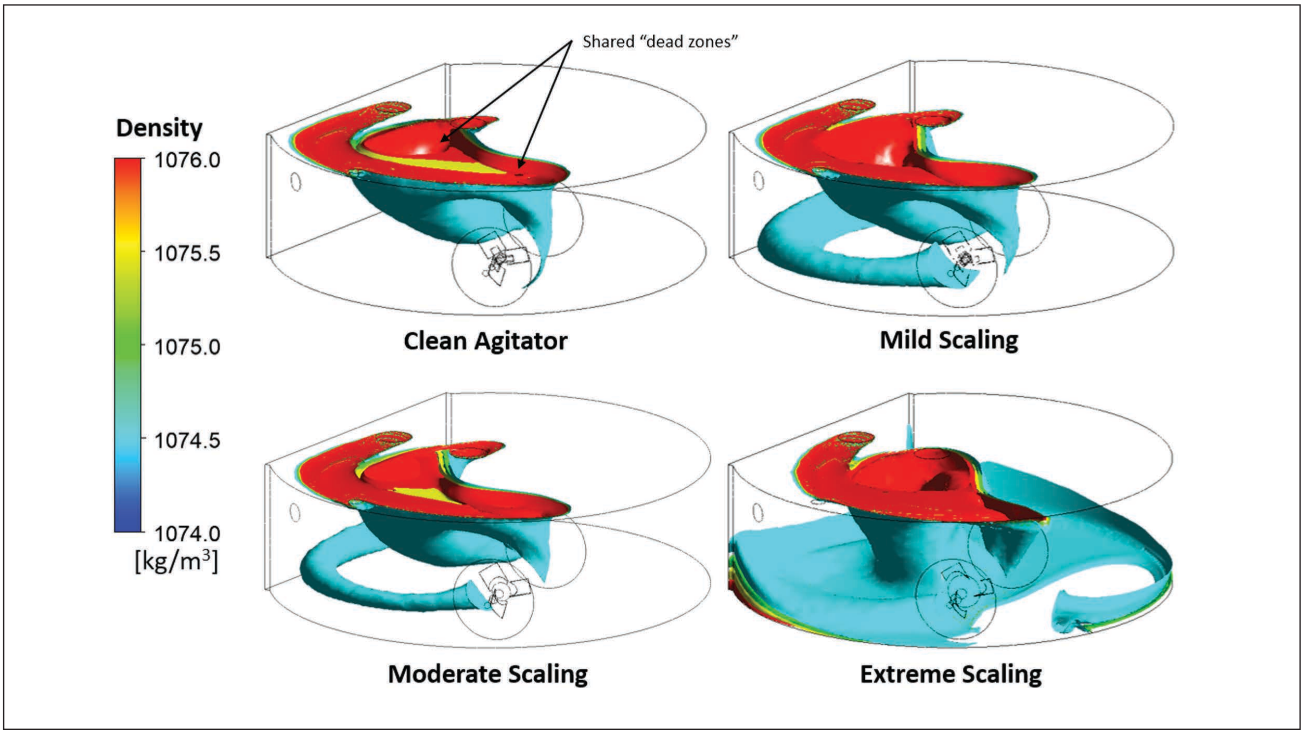

16. Isosurfaces of above average density in the tank due to higher smelt concentration.

Effects on smelt mixing

The multiphase model tracked the volume fractions of the smelt and weak wash phases throughout the tank, and overall densities were computed based on the volume fractions. Since smelt is denser than weak wash, higher smelt concentrations are denoted by regions of higher overall density. The average overall density in the tank is 1074.4 kg/m^3 for all the cases, and the resulting variances are very small due to the long residence times and considerable agitation. Four density isosurfaces, corresponding to 1074.5, 1075, 1075.5, and 1076.0 kg/m^3, allow for visualization of the extent of mixing of the weak wash and smelt in all cases (**Fig. 16**). Regions encapsulated by these surfaces have higher smelt concentrations. Near the smelt inlets, smelt concentration is obviously highest. The recirculated flow from the jets then sweeps the smelt towards the agitators and into "dead zones" that are shared by all four cases. These dead zones thus have higher smelt concentrations, which coincide with the findings of Cho [4]. The bottom of the tank has higher smelt concentrations for all three scaling cases, but this is especially pronounced for the extreme scaling case. Acknowledging that smelt-water interaction is more complicated than modeled here and thus actual smelt concentrations might look somewhat different, the results nevertheless indicate that in the extreme scaling case, mixing of smelt with weak wash is diminished, which may imply a risk of smelt pooling.

CONCLUSIONS

The results presented in this paper strongly indicate that by the time an agitator scales to the degree that it needs to be taken down due to excessive vibration or the limitations of pump amps, it is likely no longer mixing sufficiently. What is harder to quantify is when mixing is no longer adequate between the moderate case and extreme case. The next step in this research will be to better account for smelt-water interaction, including smelt droplet cooling and dissolution, which will better define the conditions for which smelt droplets begin to reach the bottom of the tank and pool, rather than dissolve. Additional modeling work is also needed to better understand what limits the strength of the jet so that some more general guidelines on agitator scaling can be provided. Lastly, additional modeling work is needed to identify the source of the oscillations seen in the mild and moderate scaling cases.

ABOUT THIS PAPER

Cite this article as:
Gareau, P., Bussmann, M., and DeMartini, N., *TAPPI J.* 21(4): 189(2022). https://doi.org/10.32964/TJ21.4.189

DOI: https://doi.org/10.32964/TJ21.4.189

ISSN: 0734-1415

Publisher: TAPPI Press

About this journal

ACKNOWLEDGEMENTS

This work is part of the industrial research consortium project Effective Energy and Chemical Recovery in Pulp and Paper Mills - III at the University of Toronto supported by Andritz, Arauco, Babcock & Wilcox, Canadian Kraft Paper, Cenibra, Clyde Bergemann, CMPC, FITNIR, FPInnovations, Georgia Pacific, International Paper, Irving, KFS, Klabin, Mercer, Rayonier, Sappi, Södra, Stora Enso, Suzano, Valmet, and WestRock. We would also like to acknowledge

ABOUT THE AUTHORS

Hard calcium carbonate scale often forms on the agitators in smelt dissolving tanks, and the effects of this scale on mixing are not well understood. A steady state, 3D model has been developed for a smelt dissolving tank at a kraft pulp mill to better understand the impact of agitator scaling on hydrodynamics and tank concentrations. While mixing in tanks has often been modeled in the literature, there have been no studies involving agitator scaling.

Modeling mixing in an industrial-scale tank is computationally expensive. Thus, finding the right balance between model accuracy and computational expense was the most difficult aspect of this research, which was addressed through a literature review of other mixing tank models and by trying different models during the model development stage.

Flow fields were obtained for four cases (clean agitators and mild, moderate, and extreme scaling), showing that mixing is negatively impacted by agitator scaling, particularly for the extreme scaling case, in which a 35% reduction in the average fluid velocity in the tank resulted.

The results presented in this paper strongly indicate that by the time an agitator scales to the degree that it needs to be taken down due to excessive vibration or the limitations of pump amps, it is likely no longer mixing sufficiently, which may lead to smelt pooling. With the information presented here,

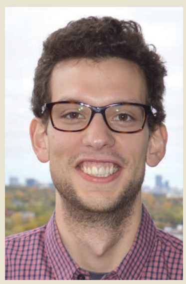

Gareau

Bussmann

DeMartini

mills can have better knowledge of the degree to which mixing is impacted by agitator scaling and when it needs to be shut down for removal and cleaning. The next step in this research will be to better account for smelt-water interaction, including smelt droplet cooling and dissolution, which will better define the conditions for which smelt droplets begin to reach the bottom of the tank and pool, rather than dissolve.

Gareau is an MASc graduate and Bussmann is professor and chair of the Department of Mechanical & Industrial Engineering at the University of Toronto, Toronto, Canada. DeMartini is associate professor in the Department of Chemical Engineering & Applied Chemistry at the University of Toronto, Toronto, Canada. Email Bussmann at markus.bussmann@utoronto.ca.

the support of the Natural Sciences and Engineering Research Council of Canada (NSERC), [IRCPJ 517715 -16]. Cette recherche a été financée par le Conseil de recherches en sciences naturelles et en génie du Canada (CRSNG), [IRCPJ 517715 -16].

LITERATURE CITED

1. Giglio, A., Björk, M., Wadsborn, R., et al., *TAPPI J.* 19(8): 387(2020). https://doi.org/10.32964/TJ19.8.387.
2. Jin, E., Bussmann, M., and Tran, H., *TAPPI J.* 14(6): 385(2015). https://doi.org/10.32964/TJ14.6.385.
3. Jin, E., "Smelt droplet-water interaction in the kraft recovery boiler dissolving tank," Ph.D. thesis, University of Toronto, Toronto, 2017.
4. Cho, D., "Computational fluid dynamics modeling of dissolving tank hydrodynamics," MASc thesis, University of Toronto, Toronto, 2020.
5. Torotwa, I. and Ji, C., *Designs* 2(1): 2010010(2018). https://doi.org/10.3390/designs2010010.
6. Zamankhan, P., *Chem. Eng. Technol.* 33(3): 508(2010). https://doi.org/10.1002/ceat.200900347.
7. Cao, H., Amador, C., Jia, X., et al., *Chem. Eng. Res. Des.* 114: 108(2016). https://doi.org/10.1016/j.cherd.2016.08.012.
8. Pakzad, L., Ein-Mozaffari, F., Upreti, S.R., et al., *Can. J. Chem. Eng.* 91: 90(2013). https://doi.org/10.1002/cjce.21616.
9. Zadravec, M., Basic, S., and Hribersek, M., *J. Eng. Sci. Technol.* 2(2): 126(2007).
10. Madhania, S., Cahyani, A.B., Nurtono, T., et al., *IOP Conf. Ser.: Mater. Sci. Eng.* 316: 012014(2018). https://doi.org/10.1088/1757-899X/316/1/012014.
11. Hernández-Jaramillo, D.C., Nieto-Londoño, C., Álvarez-Sarmiento, N., et al., *Iteckne* 12(1): 25(2014). https://doi.org/10.15332/iteckne.v12i1.818.
12. Madhania, S., Fathonah, N.N., Kusdianto, et al., *MATEC Web Conf.* 333: 02003(2021). https://doi.org/10.1051/matecconf/202133302003.
13. ANSYS, "Chapter 9: Modeling flows with moving reference frames," in *ANSYS Fluent, 19.1, Help System, User Guide*, ANSYS Inc., Canonsburg, PA, USA, 2019, pp. 997-1020.
14. ANSYS, "Chapter 10: Modeling flows using sliding and dynamic meshes," in *ANSYS Fluent, 19.1, Help System, User Guide*, ANSYS Inc., Canonsburg, PA, USA, 2019, pp. 1021-1142.
15. Lin, Z., "Characterizing smelt shattering in recovery boilers," Ph.D. thesis, University of Toronto, Toronto, 2014.
16. ANSYS, "Chapter 4: Turbulence," in *ANSYS Fluent, 19.1, Help System, Theory Guide*, ANSYS Inc., Canonsburg, PA, USA, 2019, pp. 39-140.
17. ANSYS, "Chapter 17: Multiphase flows," in A*NSYS Fluent, 19.1, Help System, Theory Guide*, ANSYS Inc., Canonsburg, PA, USA, 2019, pp. 505-652.
18. ANSYS, "Chapter 21: Solver theory," in *ANSYS Fluent, 19.1, Help System, Theory Guide*, ANSYS Inc., 2019, pp. 679-740.
19. ANSYS, "Chapter 17: Generating polyhedral meshes," in *ANSYS Fluent, 19.1, Help System, User Guide*, ANSYS Inc., Canonsburg, PA, USA, 2019, pp. 267-272.